Modified MATPOWER for Multi-Period Power Flow Analysis with PV Integration

Noppanut Chitgreeyan[1], Pongsuk Pilalum[1], Yuttana Kongjeen[1,*], Rungphet Kongnok[1], Krittidet Buayai[1], and Kaan Kerdchuen[1]

ARTICLE INFO

Article history:
Received: 19 June 2023
Revised: 15 September 2023
Accepted: 24 January 2024
Online: 20 June 2024

Keywords:
Energy demand
Energy loss
MATPOWER program
Multi-period
Power flow analysis
Photovoltaic system
Voltage stability index

ABSTRACT

The traditional power flow analysis utilizes a static state power flow with a peak load value. However, real-world scenarios demand rapid responses to fluctuations in system loading and associated time periods. As a result, the MATPOWER program is modified to solve the power flow analysis from a steady state to multi-period. This analysis involves solving the power flow over a given time scale. This paper employed energy demand and photovoltaic (PV) system profiles to implement the power flow analysis on the grid. For this purpose, the IEEE 33 bus radial distribution system was adapted. The multi-period power system analysis was categorized into two distinct cases. The penetration levels of loads and PV installations, which highlighted the analysis of power system loss and the voltage stability index for the electrical power system. The simulation results indicated that higher load penetration levels significantly influenced energy loss, a factor that was superior to the impact on the voltage stability of the grid. Notably, in Sub-Case 8, energy loss was minimized when PV was positioned in the system's high-load areas. Thus, optimal PV installation was determined by considering multi-period load and PV profiles for the power flow analysis. The yield point could be adjusted using tools from the modified MATPOWER to address power flow across multiple time periods. This yielded accurate results, as evidenced by a comparison to the DIgSILENT® program, with the base case presenting an error of 0.06%.

1. INTRODUCTION

Nowadays, the demand for electric power consumption is increasing as a result of population growth and economic expansion, which necessitates the allocation of energy sources to meet demand. Generally, electricity is generated using fossil fuels and coal non-renewable energy, which results to reduced amount of fuel, rising price of electricity, and emission of greenhouse gas (GHG) into the atmosphere. The Global Energy Perspective 2022 forecasted an increased role of renewable energy sources (RES) [1-3] such as wind power and solar energy [4]. However, the generation of renewable energy is intermittent and has a high level of output uncertainty. Also, the modern loads connected to the power system change according to energy consumption behavior. These factors contribute to the complexity of power system management. Therefore, power system planning should use comprehensive simulation and analysis tools.

Many researchers have used computer programming techniques to analyze the problems of electrical power systems [5], such as power flow analysis (PF) [6], continuation power flow (CPF) [7], small signal stability analysis (SSSA) [8], electromagnetic transient (EMT), time domain simulation (TDS), unbalanced power flow analysis (UPF) [9], quasi-dynamic simulation (QDS) [10, 11], and Graphic user interfaces (GUI). Currently, there are various types of software for analyzing electrical systems and many ways of selecting one for solving optimization problems. Basically, the analysis of electrical power systems using computer programs can be used to solve complicated problems and improve the computational speed of numerical methods. DIgSILENT® [12] program is a commercial software that is widely used because it is able to analyze electrical power systems in many methods [13] with high accuracy and flexibility. Meanwhile, open -source software is widely used by researchers for power system analysis because it can be modified and adapted for each problem. Open distribution system simulator (OpenDSS) [14], power system analysis toolbox (PSAT), and MATPOWER [15] are freeware that are popularly used in the present. However, the MATPOWER program needs to be used by interfacing it with the MATLAB program. The MATPOWER has library support for analyzing the electrical power system. Commonly, electrical power system analysis is used to

[1]*Department of Electrical engineering, Faculty of Engineering and Technology, Rajamangala University of Technology Isan, Nakhonratchasima, Thailand.*
**Corresponding author:* Yuttana Kongjeen; Phone: +66- 44-233-000; Email: yuttana.ko@rmuti.ac.th.

improve many problems, such as electrical power system loss [16], system voltage [17, 18], and power system stability [7]. The electrical power system can be significantly improved using capacitors, feeder reconfigurations, or distributed generators (DGs) as presented in Refs. [19-21],. However, the MATPOWER can only analyze the power system under static power flow. Meanwhile, the modern power flow analysis considers the changes in the energy behavior of the power system in the time periods. This paper enhanced MATPOWER to address multi-period power flow, closely mirroring the actual power demand consumption of the grid. The objectives of this study include:

1. Adapting the balanced steady-state power flow in MATPOWER to facilitate multi-period analysis.

2. Investigating the impact of load on power systems by contrasting multi-period analysis with steady-state analysis.

3. Highlighting the enhancement in voltage stability when distributed generators, specifically solar power plant is integrated.

This paper is organized into five parts. The first section presents the introduction. The second section explains the modified power flow analysis for multi-period. The third section describes the methodology. The fourth section illustrates the simulation results. And, the final section reveals the conclusion.

2. MODIFIED POWER FLOW ANALYSIS FOR MULTI-PERIOD

2.1. Newton-Raphson power flow

The traditional power flow (PF) in electrical power systems can be calculated using the Newton-Raphson power flow (NRPF) method. This method employs an admittance bus matrix, which is based on the transmission line model of the electrical power system. Power flow analysis involves solving nonlinear equations using Taylor's series, which is recognized for its superior convergence properties. While PF is typically used for steady-state load purposes, modern electrical power systems now incorporate contemporary loads influenced by evolving energy consumption behaviors. This energy consumption is often delineated by time periods, which can be further subdivided into multiple periods. Typically, a day is divided into 96 periods, a standard derived from the energy meters used by electricity providers. As such, the modified power flow analysis (MPFA) has been developed to integrate the NRPF with this multi-period framework. The MPFA accounts for transmission line current, active power, and reactive power, as detailed in [22] and presented in Equations (1) to (3).

$$I_i^t = \sum_{j=1}^{n} Y_{ij} V_j^t = \sum_{j=1}^{n} \left|Y_{ij}\right|\left|V_j^t\right| \angle(\theta_{ij} + \delta_j^t) \tag{1}$$

$$P_i^t = \sum_{j=1}^{N} \left|V_i^t\right|\left|V_j^t\right|\left(G_{ij}\cos\left(\delta_i - \delta_j\right) + B_{ij}\sin\left(\delta_i - \delta_j\right)\right) \tag{2}$$

$$Q_i^t = \sum_{j=1}^{N} \left|V_i^t\right|\left|V_j^t\right|\left(G_{ij}\sin\left(\delta_i - \delta_j\right) - B_{ij}\cos\left(\delta_i - \delta_j\right)\right) \tag{3}$$

where, I is the transmission line injection current, V is the bus voltage magnitude, θ is the transmission line impedance angle, δ is the bus voltage angle, P is the bus real power, Q is the bus reactive power, i, j are the bus or branch, n is number of transmission line, N is number of bus and t is the time in periods.

2.2. Power and energy balance solution

The constraints are represented by the load flow equations, which ensure system balance and are depicted in Equations (4) and (5). The system's inequality constraints are outlined in Equations (6) and (7); these set the limits for control variables, including the power limits of PV, the voltage magnitude limits of the bus, and the reverse power flow (RPF) limit [23].

$$P_{grid}^t - P_{PV}^t - P_{load}^t - P_{loss}^t = 0 \tag{4}$$

$$\begin{aligned} &\int_0^{N=period} P_{grid}^t dt - \int_{N=start}^{N=stop} P_{PV}^t dt - \dots \\ &\int_0^{N=period} P_{load}^t dt - \int_0^{N=period} P_{loss}^t dt = 0 \end{aligned} \tag{5}$$

$$\left.\begin{aligned} P_{PV(i),min}^t \le P_{PV(i)}^t \le P_{PV(i),max}^t \\ \left|V_{(i)}\right|_{min} \le \left|V_{(i)}\right| \le \left|V_{(i)}\right|_{max} \end{aligned}\right\} i \in Bus\ \ No. \tag{6}$$

$$P_{RPF}^t \le 0 \tag{7}$$

where, P_{grid} is the grid power injection, P_{PV} is the PV power generation, P_{loss} is the real power loss of the system, V is voltage magnitude at bus i, P_{RPF} is the reverse power flow, and t is the time in periods.

2.3. Load modelling

The constant power load model represents both the real and reactive power consumption. While load power demand is typically defined by the peak load level, the MPFA accounts for multi-periods, reflecting the energy consumption behavior. This model is described in Equations (8) to (9) [22].

$$s_d^i = p_d^i + jq_d^i \tag{8}$$

$$\left[\mathbf{s}_d^i\right] = \left[\mathbf{p}_d^i + j\mathbf{q}_d^i\right]\left[\mathbf{p}_{d,pu}^t \quad \mathbf{q}_{d,pu}^t\right]\ ;\ t \forall N \tag{9}$$

where, $\boldsymbol{s}_d$ is the apparent power of load, $\boldsymbol{p}_d$ is the real power of load, $\boldsymbol{q}_d$ is the reactive power of load, i is the bus number, N is number of periods and t is the time in periods.

The energy consumption behavior is used in the modeling of loads that have been divided by using the energy consumption during the time of day, the seasonal

variation, or the type of consumers [10, 24]. These are used to study load behavior in many studies. This paper used consumer types based on residential, commercial, and industrial loads. The energy demand of load is divided by using data from the Provincial Electricity Authority (PEA) in Thailand to study the characteristics of electricity consumption [25]. The residential load indicates peak demand at night. The commercial load indicates peak demand during the day. The industrial load indicates peak demand throughout the day. The loads profiles are shown in Fig. 1 as follows.

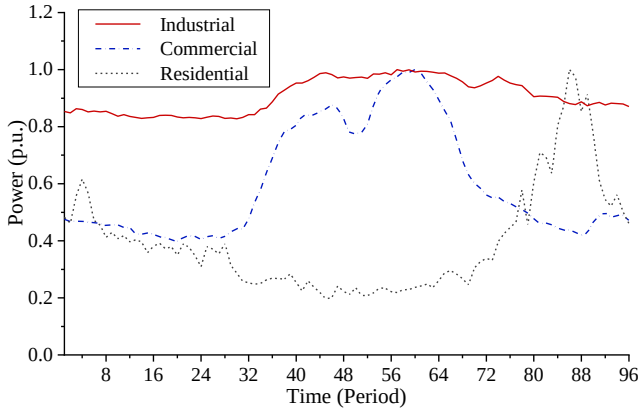

Fig. 1. Power magnitude profiles of loads.

2.4. Integration of photovoltaic system in electrical power system

The photovoltaic system (PV) is a type of distributed generator (DG), which can be categorized into four types [21]. The first type injects constant real power (P) only. The second type injects constant real and reactive power (P, Q). The third type injects constant real power (P) but consumes reactive power (Q). The final type delivers reactive power (Q) only. The DG of the NRPF can be represented by Equations (10) to (11) as follows [22].

$$s_g^i = p_g^i + jq_g^i \tag{10}$$

$$\left[\mathbf{s}_g^i\right] = \left[\mathbf{p}_g^i + j\mathbf{q}_g^i\right]\left[\mathbf{p}_{g,pu}^t\right] \;;\; t \forall N \tag{11}$$

where, $\boldsymbol{s}_g$ is the apparent power of generator, $\boldsymbol{p}_g$ is the real power of generator, $\boldsymbol{q}_g$ is the reactive power of generator, i is the bus number, N is number of periods and t is the time in periods.

A PV, also known as a solar panel, generates electrical power that is conveyed via the direct current bus. An inverter manages the energy, facilitating its conversion from direct current (DC) to alternating current (AC). This energy is then transmitted using a transmission line and a step-up transformer, which connects to the grid at the point of common coupling (PCC). Fig. 2 shows a block diagram illustrating the PV's connection to the grid , with the relevant equations provided from (12) to (13) [26].

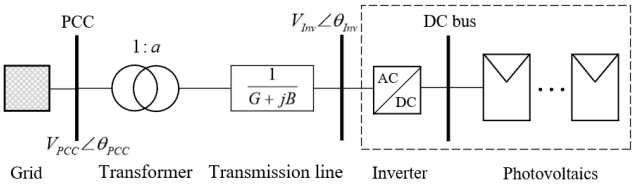

Fig. 2. Block diagram of the PV.

$$P_{PV} = V_{Inv}V_{PCC}\begin{bmatrix} G\cos\left(\theta_{Inv} - \theta_{PCC}\right) + \ldots \\ B\sin\left(\theta_{Inv} - \theta_{PCC}\right) \end{bmatrix} \tag{12}$$

$$Q_{PV} = P_{PV}\tan\left(\theta_{Inv} - \theta_{PCC}\right) \tag{13}$$

where, V_{PV} is the PV output voltage, V_{Inv} is the inverter output voltage, V_{PCC} is the bus voltage, G is the line equivalent conductance, B is the line equivalent susceptance and P_{PV}, Q_{PV} are the rated real and reactive power of PV, respectively.

Normally, PV produces energy when the sunlight is sufficient [27]. The power generation of PV is described in Fig. 3, which presents the power profiles of the PV. The PV power generation can be simulated from the twenty-fourth period (6:00 AM) to the seventy-third period (6:00 PM), which are daytime periods.

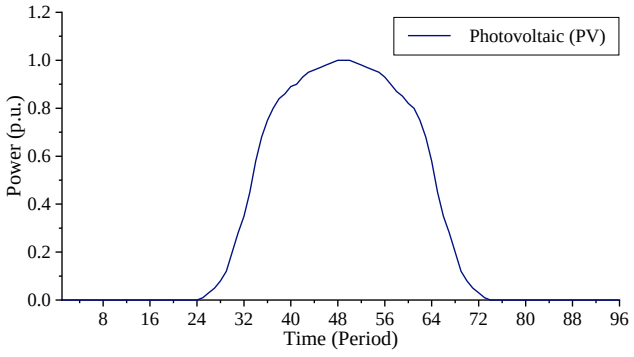

Fig. 3. Power profiles of the PV.

2.5. Total power and energy loss system formulation

The system loss can be evaluated by examining the difference in power injection at buses i and j, as illustrated in Fig. 4. Power loss is assessed based on the real power loss in the transmission line during steady-state operation. This loss can be evaluated at peak load times. When integrating power flow analysis with multi-period considerations, the total energy loss is represented as system loss. This is calculated using the real power loss at each time interval. This is further detailed in Equations (14) to (18) [28].

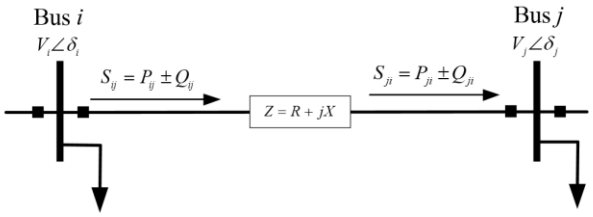

Fig. 4. Two bus equivalent circuit for power and energy loss, VDI and FVSI

$$S_{ij}^t = V_i^t I_{ij}^{t\,*} \tag{14}$$

$$S_{ji}^t = V_j^t I_{ji}^{t\,*} \tag{15}$$

$$S_{loss,ij}^t = S_{ij}^t + S_{ji}^t \tag{16}$$

$$P_{loss,total} = \text{Real}\left(S_{loss,ij}^t\right)\ ;\ t\forall N \tag{17}$$

$$E_{loss} = \int_{t-1}^{t} P_{loss,total}(t)dt \tag{18}$$

where, S_{loss} is power loss in transmission line (ij), P_{loss} is the real power loss of the system, E_{loss} is the energy loss of the system and t is the time in periods.

2.6. Voltage deviation index

The Voltage Deviation Index (VDI) is an index for assessing bus voltage stability. It is calculated by determining the difference between the voltage at a reference bus and the voltage magnitude at any other bus. Minimizing the VDI helps in illustrating the voltage violations within the power system. While the VDI in steady-state can typically serve as the PF when considering power demand at peak load levels, there are also multi-period VDI values that encompass maximum, average, and minimum readings. Figure 4 and Equations (19) to (20) detail the representation of the VDI [29].

$$VDI^t = \sum_{k=2}^{n}\left(V_k^{ref} - V_k^t\right)\ ;\ t\forall N \tag{19}$$

$$VDI_{max,mean,min} = \left[\mathbf{VDI}^t\right] \tag{20}$$

where, V_k^{ref} is the voltage at reference bus which is set to 1 p.u., V_k is the voltage at another bus, n is the number of bus and t is the time in periods.

2.7. Fast voltage stability index

The fast voltage stability index (FVSI) is a line voltage stability index that is proposed as an index for the voltage collapse or critical point of the system. The FVSI is considered by using the line impedance, the reactive power flow to the receiving bus, and the voltage at the sending bus. Normally, the FVSI must be less than 1 to ensure that the power system remains stable. So, the multi-period approach should be used for the maximum FVSI that can show the highest impact of the electrical power system. The FVSI is presented in Fig. 4 and Equations (21) to (22) as follows [6].

$$FVSI = \max\left(\frac{4Z^2Q_{ji}^t}{V_i^{t2}X}\right)\ ;\ t\forall N \tag{21}$$

$$FVSI_{max,mean,min} = \left[\mathbf{FVSI}^t\right] \tag{22}$$

where, Z is the line impedance, X is the line reactance, Q_j is the reactive power flow at the receiving bus, V_i is the sending end voltage and t is the time in periods.

2.8. Load penetration level

The load penetration level represents the load connected to the Primary Distribution System (PDS), which is determined using the load demand of both the base case and each subsequent case. This is illustrated in Equation (23) [30].

$$Penetration\ level(\%) = \frac{\sum P_{D,new}}{\sum P_{D,base}} \times 100 \tag{23}$$

where, $P_{D,new}$ and $P_{D,base}$ are the real power demand of load, respectively.

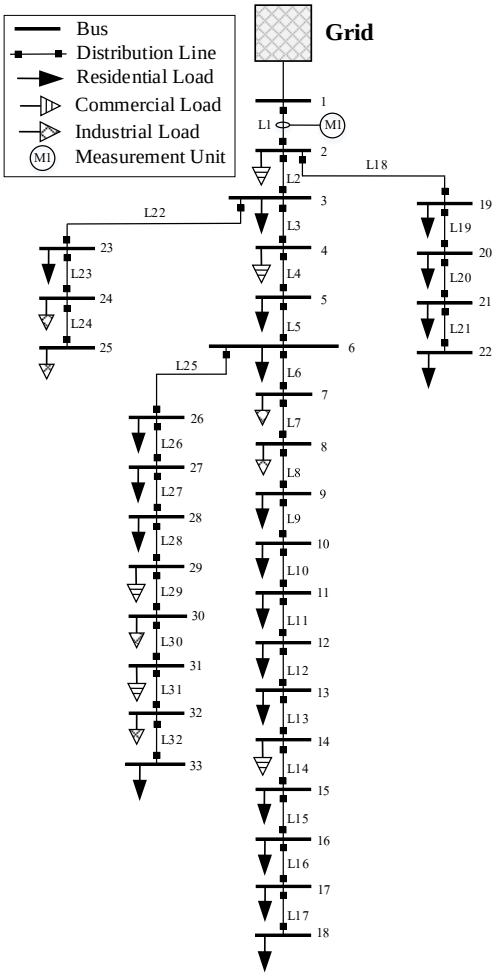

Fig. 5. The IEEE 33 bus testing system integrated with multi-period of loads.

3. METHODOLOGY

3.1. Loads classification

As illustrated in Fig. 5, the Power Distribution System (PDS) was evaluated using the IEEE 33-bus radial distribution system. This system encompassed 32 transmission lines, which carried a total load of 3.72 MW and 2.30 MVar [18]. The chosen load classification ensures that the load at any bus can be depicted by Equation (24).

$$Load\ Type = \begin{cases} P_D \geq 200kW & Industrial \\ 100kW < P_D < 200kW & Commercial \\ P_D \leq 100kW & Residential \end{cases} \quad (24)$$

where, P_D is the real power demand of load in any bus.

3.2. Study case

This research is divided into two case studies as follows:

Case I: This case examined the impact of load penetration levels, which were defined by an increase ranging from 5% to 70%. The power flow analysis considered both steady-state and multi-period loads.

Case II: This case focused on multi-period power flow with PV integration, which was defined based on various criteria: the root bus, the central point of the system, the end bus, and the heavy load.

The MPFA for multi-period was divided into seven steps. The MPFA process consisted of the input data of the radial distribution system, loads, and PV. The time scale of the period (*N*) was defined by considering the loads and PV data in 96 periods per day. The loads and PV profiles were used to update the power magnitude at any time (period). The NRPF was used to calculate the voltage magnitude and voltage angle of the system. The pseudo-code of the MPFA can be described as follows.

Pseudo-code: modified power flow analysis for multi-period

Step 1: Input data

The IEEE 33 bus with radial distribution system is shown in Fig. 6.

The load profiles are represented in Fig. 2.

The PV profiles are represented in Fig. 3 and 4.

Step 2: Defining the time scale of periods *N* (24, 48 or 96)

Step 3: for *t = 1...N*

Updating load demand $\mathbf{p}^t_{d,pu}$ and $\mathbf{q}^t_{d,pu}$ by using Equation (9).

Updating PV injection $\mathbf{p}^t_{g,pu}$ by using Equation (11).

Step 4: if $0.1 \leq p^t_{g,pu} \leq 1.0$

Installing PV by using Equations (12) and (13).

else

Calculating the PF of any period *t* by using Equations (1) to (3).

End

Step 5: Calculating the voltage magnitude and voltage angle of the system. Calculating the total power loss, the VDI and the FVSI by using Equations (17), (19) and (21).

Step 6: Return if $t < N$ to **step 3**

else break end

Step 7: Calculating the energy loss of the system by using Equation (18).

The VDI and the FVSI are considered by using Equations (20) and (22).

Consequently, scenarios for testing the system were established by determining the size and location of the PV, which resulted in 20 sub-cases. The size of the PV was defined by the power and energy balance at the point of common coupling (PCC), which highlighted the differences in sizes between static and multi-period stages. Table 1 provides further details.

Table 1. Scenarios for analyzing the PDS for PV installation

Location area	Sub-Case (No.)	Photovoltaic system	
		Position (Bus)	Sizing (MW)
-	Base Case	Without PV	
Root bus	1,5,9,13,17	2	1, 1.5, 2, 2.5, 3
Center point	2,6,10,14,18	6	
End bus	3,7,11,15,19	18	
Heavy load	4,8,12,16,20	30	

4. RESULTS AND DISCUSION

In this section, the simulation results of the modified power flow analysis for multi-period energy demand were integrated with the PV. The results were divided into two parts. The first section discusses the impact of load penetration levels on the PDS. The second section discusses the PDS when the PV was installed. The simulation results were verified by using DIgSILENT® program. Table 2. shows the comparison of simulation results from base case. The percentage error of energy loss remained at about 0.06 %, which is an acceptable value for verifying the results of modified MATPOWER.

Table 2. Comparison of energy loss simulation results

Software	Energy loss (kWh)
DIgSILENT®	8968.392
MATPOWER	8973.833
Error (%)	0.060

Table 3. Impact of load penetration levels of Case I

Load penetration level (%)	Steady-state			Modified power flow analysis with multi-period system without PV						
	Ploss	VDI	FVSI	Eloss	VDI, max	VDI, avg	VDI, min	FVSI, max	FVSI, avg	FVSI, min
	(MW)	(%)	(%)	(MWh)	(%)	(%)	(%)	(%)	(%)	(%)
0 (base case)	0.2027	1.7009	0.6709	8.9738	1.4230	1.0872	0.8912	0.5586	0.4875	0.4187
5	0.2252	1.7933	0.7081	9.9439	1.4990	1.1445	0.9377	0.5880	0.5128	0.4402
10	0.2492	1.8865	0.7458	10.9693	1.5756	1.2021	0.9845	0.6181	0.5382	0.4619
15	0.2746	1.9805	0.7838	12.4941	1.6527	1.2601	1.0314	0.6489	0.5638	0.4836
20	0.3015	2.0755	0.8223	13.6758	1.7305	1.3183	1.0785	0.6801	0.5894	0.5054
25	0.3299	2.1713	0.8613	14.9180	1.8087	1.3769	1.1258	0.7115	0.6152	0.5272
30	0.3598	2.2681	0.9007	16.2219	1.8876	1.4359	1.1734	0.7432	0.6411	0.5492
35	0.3914	2.3658	0.9406	18.5462	1.9671	1.4952	1.2212	0.7753	0.6672	0.5712
40	0.4247	2.4646	0.9810	20.0595	2.0472	1.5548	1.2692	0.8076	0.6934	0.5932
45	0.4596	2.5644	**1.0220**	21.6422	2.1280	1.6148	1.3174	0.8402	0.7197	0.6154
50	0.4964	2.6653	**1.0634**	23.2957	2.2094	1.6752	1.3658	0.8732	0.7462	0.6376
55	0.5349	2.7672	**1.1055**	25.0214	2.2915	1.7359	1.4145	0.9065	0.7729	0.6599
60	0.5754	2.8703	**1.1481**	26.8208	2.3742	1.7970	1.4634	0.9402	0.7999	0.6823
65	0.6178	2.9747	**1.1912**	28.6954	2.4577	1.8585	1.5126	0.9742	0.8272	0.7048
70	0.6622	3.0802	**1.2350**	39.4476	2.5419	1.9204	1.5620	**1.0086**	0.8549	0.7273

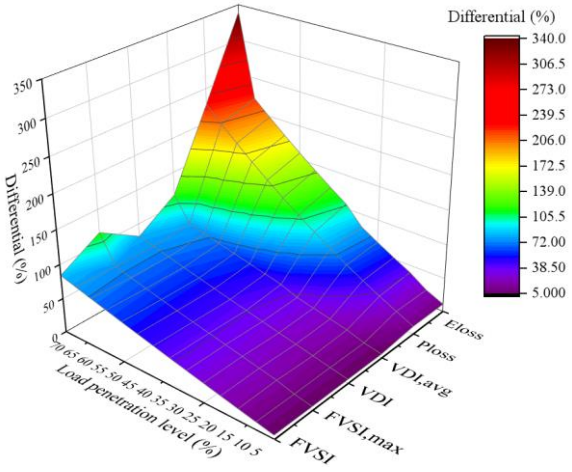

Fig. 6. The contour of the percentage difference in the total system loss VDI and FVSI.

4.1. The simulation results of Case I

The impact of load penetration levels is shown in Table 3. The penetration levels of loads were defined by increasing the range from 5 to 70 %. The impact of 70 % load penetration levels in a steady-state by using peak load profiles on the power loss, VDI, and FVSI were the highest at 0.6622 MW, 3.0802 %, and 1.2350 %, respectively. The impact of modified power flow analysis with multi-period system showed that the effect was the highest at 70 % load penetration levels. The impact on the total energy loss was 39.4476 MWh. The impact on the maximum, average, and minimum VDI were 2.5419, 1.9204, and 1.5620 %, respectively. The impact on the maximum, average, and minimum FVSI were 1.0086, 0.8549, and 0.7273 %, respectively. Therefore, the simulation results showed that the impact on the PDS increased with an increase in the penetration levels of loads.

Fig. 6 shows the contour of the percentage difference between the total system loss, VDI, and FVSI. These were the percentage difference between the base case (load penetration level at 0 %) and any case. The results showed that the impact of the percentage difference in energy and power loss was more significant than the percentage difference in VDI and FVSI. The highest percentage difference in energy and power loss was 339.58 and 226.72 %, respectively, which were the case load penetration levels at 70 %. The highest percentage differences in VDI (avg.), VDI, FVSI (max), and FVSI were 115.86, 81.08, 116.29, and 84.08 %, respectively. However, each scenario showed that the percentage difference in multi-period analysis (Eloss, VDI (avg.), and FVSI (max)) had a greater impact than the percentage difference in static state (Ploss, VDI, and FVSI).

Fig. 7 shows FVSI when installed load penetration levels. The FVSI showed that the PDS remained unstable. The

steady-state (FVSI) showed that the FVSI exceeded 1 (at 1.0220%) after the load penetration level of 45 %. However, the modified power flow analysis with multi-period system showed the FVSI (max) greater than 1 (at 1.0086 %) at the load penetration level of 70 %. As a result, when using the modified power flow analysis with multi-period system, the PDS can be supported by increasing loads, which is more than steady-state.

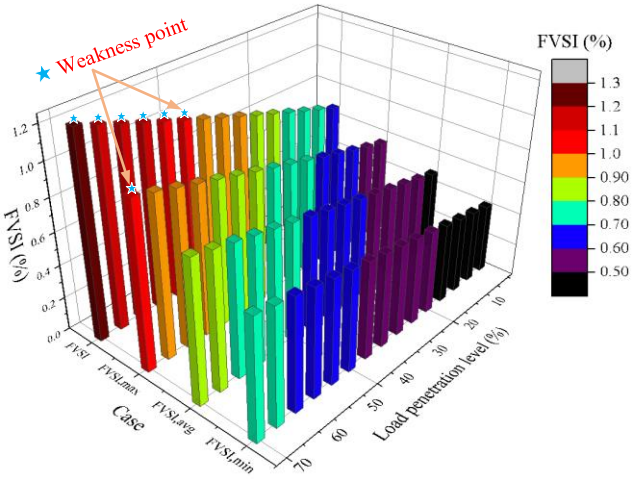

Fig. 7. Fast voltage stability index (FVSI) at different load penetration levels.

Table 4. Simulation results from each scenario for analyzing the PDS when the PV is installed

	PV		Steady-state			Modified power flow analysis with multi-period system						
	Sit	Size	Ploss	VDI	FVSI	Eloss	VDI, max	VDI, avg	VDI, min	FVSI, max	FVSI, avg	FVSI, min
Sub-Case	(Bus No.)	(MW)	(MW)	(%)	(%)	(MWh)	(%)	(%)	(%)	(%)	(%)	(%)
Base	-	-	0.2027	1.7009	0.6709	8.9738	1.4230	1.0872	0.8912	0.5586	0.4875	0.4187
1	2	1	0.2129	1.6005	0.6665	9.1030	1.4230	1.0596	0.8378	0.5586	0.4866	0.4173
2	6	1	0.1691	0.5187	1.0823	7.9831	1.4230	0.7554	0.2534	0.9916	0.5424	0.4213
3	18	1	0.1301	0.8854	0.5795	9.1440	1.4230	0.8962	0.5422	0.6551	0.5079	0.3711
4	30	1	0.0886	0.6869	0.5663	6.6353	1.4230	0.7795	0.3157	0.7794	0.4202	0.1824
5	2	1.5	0.2054	1.6005	0.6665	8.9781	1.4230	1.0596	0.8378	0.5586	0.4866	0.4173
6	6	1.5	0.1073	0.5143	0.7284	7.1664	1.4230	0.7542	0.2522	0.9487	0.4969	0.3840
7	18	1.5	0.2016	0.8648	0.7956	11.9630	1.4230	0.8917	0.5311	0.8941	0.5767	0.3708
8	30	1.5	0.0644	0.6703	0.2777	**6.6336**	1.4230	0.7753	0.3100	0.7279	0.4280	0.1617
9	2	2	0.1993	1.6005	0.6665	8.8885	1.4230	1.0596	0.8378	0.5586	0.4866	0.4173
10	6	2	0.0720	0.5103	0.4887	6.9523	1.4230	0.7532	0.2511	0.9061	0.4847	0.3666
11	18	2	0.3407	0.8624	1.0348	16.3306	1.4230	0.8916	0.5217	1.1574	0.6482	0.3706
12	30	2	0.0888	0.6599	0.4903	7.7524	1.4230	0.7726	0.3037	0.6769	0.4755	0.1805
13	2	2.5	0.1947	1.6005	0.6665	8.8341	1.4230	1.0596	0.8378	0.5586	0.4866	0.4173
14	6	2.5	**0.0615**	0.5068	0.4887	7.3049	1.4230	**0.7522**	**0.2500**	0.8637	0.4834	0.3621
15	18	2.5	0.5362	0.8752	1.2669	22.0352	1.4230	0.8951	0.5141	1.5164	0.7430	0.3720
16	30	2.5	0.1556	0.6548	0.7005	9.8728	1.4230	0.7712	0.2985	0.9497	0.5465	0.1755
17	2	3	0.1914	1.6005	0.6665	8.8147	-	-	-	-	-	-
18	6	3	0.0740	**0.5037**	0.4887	8.1924	-	-	-	-	-	-
19	18	3	0.7800	0.9010	1.5674	28.9193	-	-	-	-	-	-
20	30	3	0.2600	0.6546	0.9708	12.8983	-	-	-	-	-	-

4.2. The simulation results of Case II

The simulation results from each scenario are shown in Table 4, which have been described using the results from steady-state and modified power flow analysis with multi-period system. The power loss was minimized to 0.0615 MW in Sub-Case 14 by installing a 2.5 MW PV in bus No. 6, while the energy loss was minimized to 6.6336 MWh in Sub-Case 8 by installing a 1.5 MW PV in bus No. 30. The VDI was minimized to 0.5037 % in Sub-Case 18 by installing a 3 MW PV in bus No. 6, while VDI (avg.) was minimized to 0.7522 % in Sub-Case 14 by installing a 2.5 MW PV in bus No. 6. However, different positions of PV within the PDS must be considered when analyzing the power flow analysis for multi-periods. Therefore, the FVSI from each scenario showed that the PDS remained unstable in some scenarios. The FVSI showed that the power system was unstable in Sub-Cases 2, 11, 15, and 19 with values of 1.0823, 1.0348, 1.2669, and 1.5674 %, respectively. Moreover, the FVSI (max) greater than 1 was exhibited in Sub-Cases 11 and 15 with values of 1.1574 and 1.5164 %, respectively. Therefore, the position and size of the PV integration into the PDS should be considered as these factors affect the power system stability.

Fig. 8 shows the best case of VDI when a 3 MW PV was installed in bus No. 6 (Sub-Case 18). The voltage magnitude of the base case was minimized at bus No. 18, which was 0.9130 p.u.. As exhibited by Sub-Case 18, the PV could improve the bus voltage magnitude of the grid.

Fig. 9 shows the best case of the total power loss when a 2.5 MW PV was installed in bus No. 6 (Sub-Case 14). The transmission line loss of the base case was the highest in the root bus area because of the power transferred by bus No. 1 (slack bus). This generated energy for load demand only. Therefore, the PV at bus No. 6 could reduce the transmission line loss of the system.

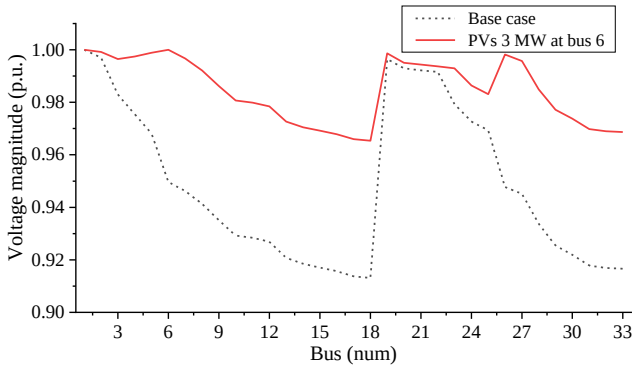

Fig. 8. Voltage magnitude profile when 3 MW PV was installed in bus No. 6 (Sub-Case 18).

Fig. 10 shows the best case of VDI (avg.) when a 2.5 MW PV was installed in bus No. 6 (Sub-Case 14). The voltage profile showed the average voltage magnitudes were improved by using the power generated by the PV from the twenty-ninth period (07.00 A.M.) to the sixty-ninth period (05.00 P.M.).

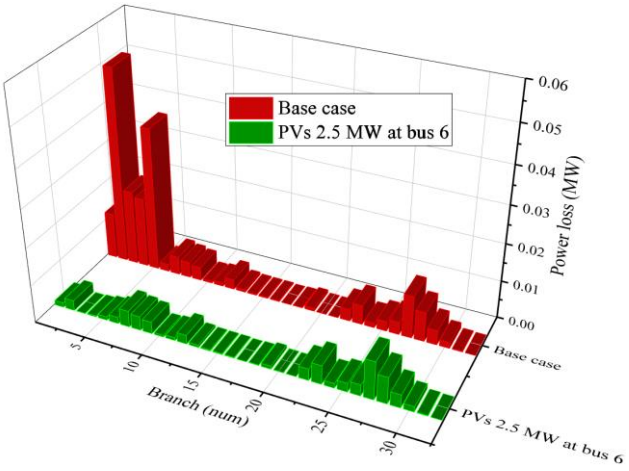

Fig. 9. Power line loss when 2.5 MW PV was installed in bus No. 6 (Sub-Case 14).

Fig. 11 shows the best case of total energy loss for when a 1.5 MW PV was installed in bus No. 30 (Sub-Case 8). When compared to the base case, the PV could reduce the total energy loss by 26.078 %.

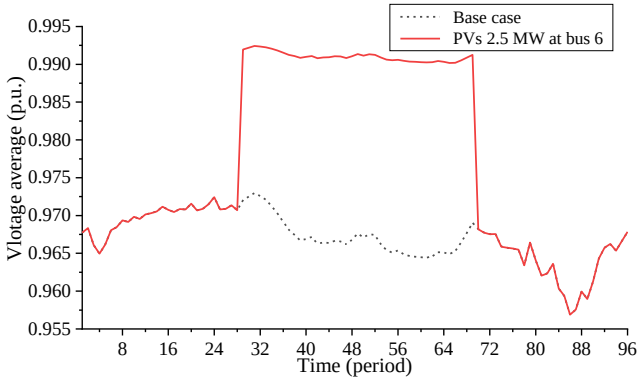

Fig. 10. Average voltage magnitude profile when a 2.5 MW PV was installed in bus No. 6 (Sub-Case 14).

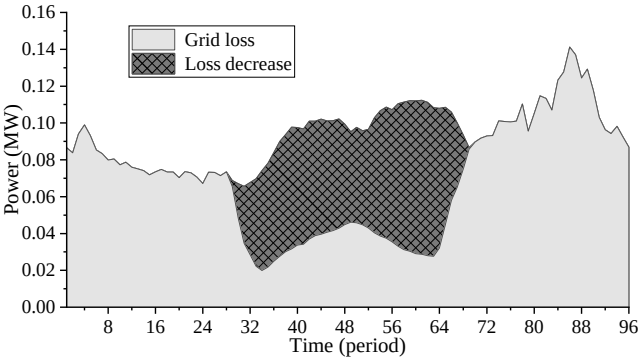

Fig. 11. Total energy loss when a 1.5 MW PV was installed in bus No. 30 (Sub-Case 8).

Fig. 12 shows the electrical power profiles when a 1.5 MW PV was installed in bus No. 30 (Sub-Case 8). The total load demand was calculated by summing the residential, commercial, and industrial loads in the power profiles, namely the camel curve. The grid injection was lower compared to the total load demand. Benchmarking of the PV generation could be supported by injecting the power generation into the grid.

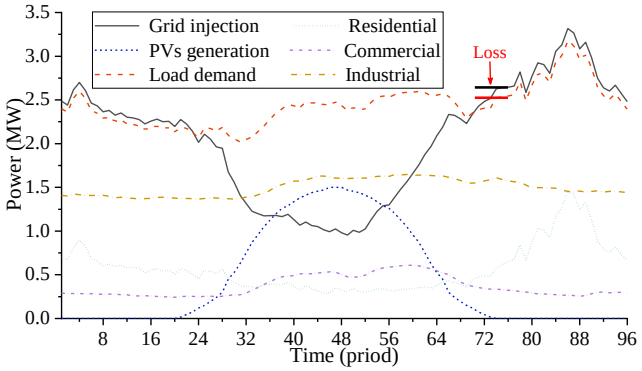

Fig. 12. Power profiles when a 1.5 MW PV was installed in bus No. 30 (Sub-Case 8).

Fig. 13 shows the grid power injection when a 1.5 MW PV was installed in bus No. 30 (Sub-Case 8). PV power generation could support grid power injection. The power injection of the system consisted of the grid injection and PV generation, which were 194.5528 (gray area) and 44.8650 (black area) MWh, respectively, which represented the percentages of 87.2607 and 18.7392 %, respectively.

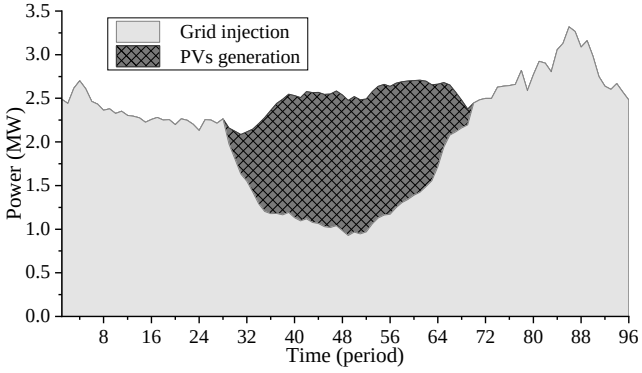

Fig. 13. Grid power injection when a 1.5 MW PV was installed in bus No. 30 (Sub-Case 8).

5. CONCLUSIONS

This paper succeeded in presenting a modified MATPOWER program to solve the balanced power flow analysis from steady state to multi-period conditions. This method is used to analyze the electrical power system conditions close to the real power system where the energy consumption changes according to consumer behaviors. The results showed that a high percentage of load penetration levels significantly affected energy loss, which exceeded the impact on the voltage stability of the electrical power system. On the other hand, the consideration of multi-period had more impact than steady state of each scenario. Improving system loss and voltage stability could be achieved by installing a distributed generator, which was the PV in this case. The power loss improvement in steady state could be achieved by installing PV at the center point of the system under single-shot power flow analysis. The power loss was lowest in Sub-Case 14, which was decreased to 0.1412 MW. Moreover, the energy loss improvement in multi-period could be achieved by installing PV at the heavy load points of the electrical power system. The energy loss is lowest in Sub-Case 8, which decreased to 2.3402 MWh. The FVSI revealed that PV installation should be in a suitable location and size to achieve power system stability when the balanced power flow analysis was considered in the steady state and the multi-period conditions. The benefits of the modified MATPOWER are that it could be suitably used to analyze power systems from the static power flow to multi-periods power flow conditions. In conclusion, this study presented a suitable PV size, RPF during peak PV power generation times was avoided and an evaluation of electrical power system.

REFERENCES

[1] Global Energy Perspective. 2022. Electrification and renewables show accelerated growth. [On-line serial], Retrieved January 10, 2023 from https: //www. mckinsey.com/ industries/oil-and-gas/our-insights/ global-energy-perspective-2022.

[2] Haegel, N. M.; and Kurtz, S. R. 2021. Global Progress Toward Renewable Electricity: Tracking the Role of Solar. IEEE Journal of Photovoltaics. vol. 11. no. 6. pp. 1335-1342. doi: 10.1109/JPHOTOV.2021.3104149.

[3] Shafiullah, M.; Ahmed, S. D.; and F. A. Al-Sulaiman. 2022. Grid Integration Challenges and Solution Strategies for Solar PV Systems: A Review. IEEE Access. vol. 10. pp. 52233-52257. doi: 10.1109/ACCESS.2022.3174555.

[4] Elavarasan, R. M. et al. 2020. A Comprehensive Review on Renewable Energy Development, Challenges, and Policies of Leading Indian States With an International Perspective. IEEE Access. vol. 8. pp. 74432-74457. doi: 10.1109/ ACCESS. 2020.2988011.

[5] De Mel, I.; Klymenko, O. V.; and M. Short. 2022. Balancing accuracy and complexity in optimisation models of distributed energy systems and microgrids with optimal power flow: A review. Sustainable Energy Technologies and Assessments. vol. 52. p. 102066. 2022/08/01/ doi: https:// doi.org/10.1016/ j.seta.2022.102066.

[6] Kongjeen, Y.; Yuakchimplee, W.; Buayai, K.; and Kerdchuen, K. 2021. Multi-objective for Re-configuration Planning in a Modern Primary Distribution System. in 2021 24th International Conference on Electrical Machines and Systems (ICEMS). 31 Oct.-3 Nov. 2021 pp. 835-839, [On-line serial], from https://ieeexplore.ieee.org/stampPDF/ getPDF.jsp?tp= &arnumber=9634501&ref=. doi: 10.23919/ ICEMS52562.2021.9634501.

[7] Liang, X.; Chai, H.; and Ravishankar, J. 2022. Analytical

Methods of Voltage Stability in Renewable Dominated Power Systems: A Review. Electricity. vol. 3. no. 1. pp. 75-107 doi: 10.3390/electricity3010006.

[8] Men, Y.; Du, Y.; and Lu, X. 2021. Distributed control framework and scalable small-signal stability analysis for dynamic microgrids. Chinese Journal of Electrical Engineering. vol. 7. no. 4. pp. 49-59. doi: 10.23919/ CJEE.2021.000037.

[9] Feizi, M. R.; Khodayar, M. E.; and Li, J. 2022. Data-driven distributionally robust unbalanced operation of distribution networks with high penetration of photovoltaic generation and electric vehicles. Electric Power Systems Research. vol. 210. p. 108001. doi: https://doi.org/10.1016/ j.epsr.2022. 108001.

[10] Gaitan, L.; Gómez, J.; and Rivas, E. 2019. Quasi-Dynamic Analysis of a Local Distribution System with Distributed Generation. Study Case: The IEEE 13 Node System. TecnoLógicas. vol. 22. pp. 195-212. doi: 10.22430/ 22565337.1489.

[11] Wynn, S. L.; Pinthurat, W.; and Marungsri, B. 2022. Multi-Objective Optimization for Peak Shaving with Demand Response under Renewable Generation Uncertainty. Energies. vol. 15. no. 23. doi: 10.3390/en15238989.

[12] DIgSILENT, GmbH. 2014. DIgSILENT PowerFactory Version 15, User Manual. INTEGRATED POWER SYSTEM ANALYSIS SOFTWARE.

[13] Adetokun, B. B.; Ojo, J. O.; and Muriithi, C. M. 2020. Reactive Power-Voltage-Based Voltage Instability Sensitivity Indices for Power Grid With Increasing Renewable Energy Penetration. IEEE Access. vol. 8. pp. 85401-85410. doi: 10.1109/ACCESS.2020.2992194.

[14] Kongjeen, Y.; Bhumkittipich, K.; and Mithulananthan, N. 2019. Optimal DG Sizing and Location in Modern Power Grids using PEVs Load Demand Probability. ECTI Transactions on Electrical Engineering, Electronics, and Communications. vol. 17. no. 1. pp. 51-59. doi: 10.37936/ecti-eec.2019171.215410.

[15] Zimmerman, R. D.; Murillo-Sánchez, C. E.; and R. J. Thomas. 2011. MATPOWER: Steady-State Operations, Planning, and Analysis Tools for Power Systems Research and Education. IEEE Transactions on Power Systems. vol. 26. no. 1. pp. 12-19. doi: 10.1109/TPWRS.2010.2051168.

[16] Kongjeen, Y.; Eiampong, W.; Buayai, K.; and Kerdchuen, K. 2023. Voltage Stability Analysis in Microgrids System with Photovoltaic Solar Energy under Uncertainty of Loads Variation. GMSARN International Journal. vol. 17. pp. 156-162.

[17] Ismail, B. et al. 2022. New Line Voltage Stability Index (BVSI) for Voltage Stability Assessment in Power System: The Comparative Studies. IEEE Access. vol. 10. pp. 103906-103931. doi: 10.1109/ACCESS.2022.3204792.

[18] Kongjeen, Y.; Bhumkittipich, K.; Mithulananthan, N.; Amiri, I. S.; and Yupapin, P. 2019. A modified backward and forward sweep method for microgrid load flow analysis under different electric vehicle load mathematical models. Electric Power Systems Research. vol. 168. pp. 46-54. doi: https://doi.org/ 10.1016/j.epsr.2018.10.031.

[19] Razavi, S. M.; Momeni, H. R.; Haghifam, M. R.; and Bolouki, S. 2022. Multi-Objective Optimization of Distribution Networks via Daily Reconfiguration. IEEE Transactions on Power Delivery. vol. 37. no. 2. pp. 775-785. doi: 10.1109/ TPWRD.2021.3070796.

[20] Purlu, M.; and Turkay, B. E. 2022. Optimal Allocation of Renewable Distributed Generations Using Heuristic Methods to Minimize Annual Energy Losses and Voltage Deviation Index. IEEE Access. vol. 10. pp. 21455-21474. doi: 10.1109/ ACCESS.2022.3153042.

[21] Leghari, Z. H.; Kumar, M.; Shaikh, P. H.; Kumar, L.; and Tran, Q. T. 2022. A Critical Review of Optimization Strategies for Simultaneous Integration of Distributed Generation and Capacitor Banks in Power Distribution Networks. Energies. vol. 15. no. 21. doi: 10.3390/en15218258.

[22] Ahmadi, A.; Smith, M. C.; Collins, E. R.; Dargahi, V.; and Jin, S. 2022. Fast Newton-Raphson Power Flow Analysis Based on Sparse Techniques and Parallel Processing. IEEE Transactions on Power Systems. vol. 37. no. 3. pp. 1695-1705. doi: 10.1109/TPWRS.2021.3116182.

[23] Unahalekhaka, P.; and Sripakarach, P. 2020. Reduction of Reverse Power Flow Using the Appropriate Size and Installation Position of a BESS for a PV Power Plant. IEEE Access. vol. 8. pp. 102897-102906. doi: 10.1109/ACCESS. 2020.2997821.

[24] Rashid, M. M. et al. 2021. Home Energy Management for Community Microgrids Using Optimal Power Sharing Algorithm. Energies. vol. 14. no. 4. doi: 10.3390/ en14041060.

[25] Provincial Electricity Authority. 2022. The study of the characteristics of electricity consumption. [On-line serial], Retrieved January 29, 2022 from http://peaoc.pea.co.th/ loadprofile/.

[26] Ai, Y.; Du, M.; Pan, Z.; and Li, G. 2021. The optimization of reactive power for distribution network with PV generation based on NSGA-III. CPSS Transactions on Power Electronics and Applications. vol. 6. no. 3. pp. 193-200. doi: 10.24295/CPSSTPEA.2021.00017.

[27] Alvarado-Barrios, L.; Rodríguez del Nozal, A.; Tapia, A.; J. Martínez-Ramos, L.; and Reina, D. G. 2019. An Evolutionary Computational Approach for the Problem of Unit Commitment and Economic Dispatch in Microgrids under Several Operation Modes. Energies. vol. 12. no. 11. doi: 10.3390/en12112143.

[28] Wu, H.; Yuan, Y.; and Ma, K.; 2020. A Novel Probabilistic Method for Energy Loss Estimation Using Minimal Line Current Information. IEEE Transactions on Power Systems. vol. 35. no. 6. pp. 4928-4931. doi: 10.1109/TPWRS. 2020. 3020719.

[29] Danish, M. S. S.; Senjyu, T.; Danish, S. M. S.; Sabory, N. R.; Krishnan, N.; and Mandal, P. 2019. A Recap of Voltage Stability Indices in the Past Three Decades. Energies. vol. 12. p. 1544. doi: 10.3390/en12081544.

[30] Chitgreeyan, N.; Kongjeen, Y.; Buayai, K.; and Kerdchuen, K.; 2021. Impact of Voltage Unbalance System on Modern Microgrid System under High Penetration of Fast Charging Station. GMSARN International Journal. vol. 15. pp. 353-359.